Rheological Evolution and Crystallization Response of Molten Coal Ash Slag at High Temperatures

Wenjia Song
The State Key Laboratory of Chemical Engineering, School of Chemical Engineering, East China University of Science and Technology, Shanghai 200237, P.R. China

Dept. of Earth and Environmental Sciences, Ludwig-Maximilians University Munich, Theresienstraße 41/III, D80333, Germany

Dept. of Applied Chemistry, Chubu University, 1200 Matsumoto-Cho, Kasugai, Aichi, 487–8501, Japan

Lihua Tang and Zibin Zhu
The State Key Laboratory of Chemical Engineering, School of Chemical Engineering, East China University of Science and Technology, Shanghai 200237, P.R. China

Yoshihiko Ninomiya
Dept. of Applied Chemistry, Chubu University, 1200 Matsumoto-Cho, Kasugai, Aichi, 487–8501, Japan

DOI 10.1002/aic.14052
Published online March 5, 2013 in Wiley Online Library (wileyonlinelibrary.com)

Ash-related problems are often the main reason for entrained-flow gasifiers and boilers unscheduled shut downs. Thus, understanding the high-temperature physical properties of molten coal ash slag may enable an accurate description of the condition of ash deposition in the gasifier and boiler. The evolution of the time dependence of rheological behaviors, including the viscosity and yield stress of the molten coal ash slag containing 0–35.51 vol % crystals at decreasing temperatures (1400–1280°C) and within 1.05 × 10^5 s, were investigated. Non-Newtonian behaviors, including shear thinning, become obvious with an increasing crystal contents. The trends in the change of crystal nucleation rate in molten coal ash slag are similar with those of the growth rate. Finally, the experimental results and the crystal-size distribution method are used to develop a semiempirical parameterization that describes the complex non-Newtonian rheology of crystal-bearing molten coal ash slag. © 2013 American Institute of Chemical Engineers *AIChE J*, 59: 2726–2742, 2013
Keywords: coal gasification, coal combustion, coal ash slag

Introduction

Coal has been and will continue to be one of the major energy resources because of its abundant reserves and competitively low prices, especially for the use of base-load power generation. For example, it contributed about 45% of the total global electricity in 2011.[1] Power plants are responsible for more than one-third of the CO_2 emissions worldwide, which effect an increase in the average global temperature. Carbon capture and storage (CCS), which is a critical technology for reducing greenhouse gas emissions, is being considered as a strategy for stabilizing the atmospheric CO_2 concentrations.[2] Capturing CO_2 from the mixed-gas streams produced during power generation is the first and critical step for CCS. Three strategies for incorporating capture into power generation scenarios, namely, precombustion capture, post combustion capture, and oxy-fuel combustion capture, are of primary focus today.[3,4] Precombustion and oxy-fuel combustion capture systems use entrained flow gasifiers (EFGs) and oxy-fuel boilers (OFBs), respectively, to gasify and combust pulverized coal.[5,6]

Generally, during the gasification and combustion of coal in EFGs and OFBs, the pulverized coal is gasified or combusted, its mineral content is converted into ash, and the ash products form a slag layer that flows down the refractory wall under gravity and out of the bottom of the furnace into a water quenching system.[7] This phenomenon is generally described as slagging (if the deposit is in a molten or viscous state).[8] The slagging of coal ash are very complex phenomena and are responsible for costly maintenance problems, as well as a reduction in heat transfer, debating during the post combustion heating and cooling processes, and some instances of unscheduled shutdowns.[9] Therefore, the slagging of coal ash must be characterized to ensure the continuous operation of EFGs and OFBs in the typical operated temperature range of 1300–1800°C during coal combustion and gasification.[10]

One of the high-temperatures physical properties of molten coal ash slag, namely, rheological behavior, is recognized as a critical factor in controlling the slagging in the furnace.[11] For slag to flow from the furnace, it is generally accepted that the slag viscosity must be sufficiently low at

Correspondence concerning this article should be addressed to W. Song at wj.song@mail.ecust.edu.cn.

the temperature of tapping, typically less than 25 Pa s.[12] Meanwhile, to ensure reliable slag tapping, the operation temperature of the furnace should be above the temperature of critical viscosity of the slag, which is recognized as a sharp break in the viscosity vs. temperature curve.[13] If the furnace is operated at a temperature lower than that of critical viscosity of the slag, the viscosity will rapidly increase and then cause viscous and erratic slag flows from the furnace. Therefore, an important goal for the past 60 years has been to measure and model the viscosity of molten coal ash slag at high temperatures. As early as the 1960s, Boow and Watt[14–16] measured the viscosity-temperature characteristics of molten coal ash slag in a wide range of temperature (750–1600°C). In the 1980s, Schobert et al.[17,18] investigated the flow properties of bituminous coal ash slags to explain various phenomena that are related to slag flow and were qualitatively observed in pilot plant testing, so as to predict a satisfactory operation in slagging fixed-bed gasification. In the 1990s, Nowok et al.[19,20] measured the viscosity, density, and liquidus phase relations. They interpreted the phenomenon of increasing viscosity with decreasing temperature for coal ash based on changes in the local structure of the slag as a result of the growth of microphases. In 2000, Hurst et al.[21,22] performed experimental viscosity measurements over a range of slag compositions that cover the anorthite region of the fluxed Australian bituminous coal ashes. In addition, some researchers used different numerical simulations and software, such as the thermodynamic computer package FactSage, to predict the viscosity of molten coal ash slag and its behavior under different conditions.[23,24] Numerous laboratory experiments have examined the viscosity of different types of molten coal ash slag at high temperatures. However, most studies have focused on the viscosity of fully molten coal ash slag without crystal particles at equilibrium condition. In addition, a generalized method for predicting the viscosity of molten coal ash slag containing crystal particles at nonequilibrium condition has not been proposed.

At temperatures above the liquidus temperature, the viscosity of molten coal ash slag with freely suspended crystals is readily estimated from its chemical composition.[25,26] At relatively low crystal contents, molten coal ash slag can generally be approximated as a Newtonian fluid. However, at higher crystal contents, rheological behavior of molten coal ash slag is no longer that of a Newtonian fluid, but that of a non-Newtonian fluid.[27] Some studies have addressed the problem of determining the viscosity of a particle suspension of molten coal ash slag as a function of the particle concentration or fluid fraction.[28] Different models and equations are available for predicting rheology of different suspensions, including those of crystal-bearing silicates. Beginning with Einstein's work,[29] from an hydrodynamic description of the motion of small rigid spheres in a fluid, Einstein predicted that the viscosity varies with the crystal volume fraction (ϕ) according to Eq. 1

$$\eta_s = \eta_l(1+2.5\phi) \tag{1}$$

where η_s is the apparent viscosity of melt, and η_1 is the viscosity of the homogeneous melt. With some geometrical arguments, the effect of the serial-size distribution of the inclusions was taken into account by Roscoe[30] who obtained

$$\eta_s = \eta_l\left(\frac{\phi_{max}}{\phi_{max}-\phi}\right)^{2.5} \tag{2}$$

where ϕ_{max} is the maximum solid-packing fraction. This equation is called the Einstein–Roscoe model. Pinkerton et al.[31] then considered the factors of the particle-shape and size distribution using the Einstein–Roscoe model and modified to the equation as follows

$$\eta_s = \eta_l e^{\left[\left(2.5+\left(\frac{\phi}{\phi_{max}-\phi}\right)^{0.48}\right)\frac{\phi}{\phi_{max}}\right]} \tag{3}$$

However, viscosity of the molten coal ash slag is related not only to its crystal volume fraction but also to the crystal properties, including the crystal sizes and size distribution, which result from a dynamic interplay of crystal nucleation and growth;[32] these factors need to be considered in the viscosity model. Therefore, the rheological properties of molten coal ash slag at high temperatures are not only related in a complex way to degassing and the thermal history of slagging, but also to the kinetics and dynamics of crystallization. Crystallization can occur through the nucleation of new crystals, growth on existing nuclei, or through a combination of the two processes.[33] In general, nucleation is assumed to dominate when surpersaturations are high, whereas crystal growth is considered also important in systems experiencing only small deviations from equilibrium. However, because of the complexity of describing crystal nucleation and growth using classical kinetic theory, which aims at an atomistic approach, a quantitative description of the kinetics and dynamics of crystallization of the complex molten coal ash slag system is difficult to provide. In addition, amount of available information on this topic is limited. Although FactSage can calculate the crystal volume fraction in the molten coal ash slag, the program can only be applied at equilibrium condition and not at nonequilibrium condition. Therefore, in this study, the crystal-size distribution (CSD) method,[34,35] which is widely used in analyzing the nucleation and crystal growth in magma and lava, was applied to molten coal ash slag systems to clarify the relationship between the temporal change in the rheological properties and the variation in the nucleation and growth rate of crystals at high temperatures. This method provides quantitative information on crystal growth rate, nucleation density, nucleation rate, and order of the governing chemical reactions. The CSD method also obtains a quantitative measurement of crystal gain or loss over a particular size range, and thus, may be proven useful in evaluating crystallization processes of molten coal ash slag.

The rheological properties of molten coal ash slag with certain particle concentrations, with the exception of viscosity, also includes other characteristics, such as flow pattern,[36] shear thinning,[37] and eventually the onset of yield stress (i.e., minimum shear stress that initiates viscous flow).[38] Understanding the complexities of the rheology of molten coal ash slag, including ash deposition behaviors, corrosion on heat exchanger tubes, slag formation, and tapping from furnace, is the key to determining and modeling the slagging processes.[39,40] However, the rheological behavior of the molten coal ash slag is difficult to measure, and studies on these rheological properties have long been limited until the last 10 years. For example, Tonmukayakul and Nguyen[41] only

Table 1. Chemical Composition of Coal Ash

Composition	SiO_2	Al_2O_3	CaO	Fe_2O_3	MgO	TiO_2	K_2O	Na_2O
Coal ash (wt %)	31.89	25.18	30.78	7.34	1.92	1.75	0.71	0.43

studied the effect of shear rate on the shear stress and apparent viscosity of laboratory coal ash. Furthermore, the other rheological behaviors of molten coal ash slag were not considered, such as yield stress and flow pattern. However, despite these new data, the existence, significance, and importance of some rheological thresholds are still under debate, and a model for predicting the rheology of molten coal ash slag over their entire change range has yet to be proposed.

In this article, the evolution of the time dependence of rheological behaviors, including the viscosity, flow pattern, and yield stress of the molten coal ash slag containing 0–35.51 vol % crystals at decreasing temperatures (1400–1280°C) and within 1.05×10^5 s (29.2 h) was first investigated. The transition of the flow pattern from Newtonian to non-Newtonian, as well as changes in the shear-thinning and yield stress behaviors with decreasing temperature, has been described. The results of the quantitative textural data from 25 samples of quenched molten coal ash slag taken at different times and temperatures are then presented, providing this description's capability to evaluate texture-related causes of changing flow patterns. Finally, the CSD method has been applied to determine the crystal growth and nucleation rates in molten coal ash slag, and the information obtained has been used to help develop the suggested viscosity model for molten coal ash slag. The outcome of this investigation will provide an inventory of the properties of molten coal ash slag that can be used for future studies.

Experimental

Coal ash sample

One coal from Shanxi province in China was gasified in the EFG by mixing with other kinds of coal with high fusibility; the resultant coal was then used as the experimental material. The ash sample was prepared in a muffle furnace according to Chinese standard GB/T 211–2001.The chemical compositions of the coal ash as analyzed by x-ray fluorescence are shown in Table 1.

Experimental equipment and method

A high-temperature rheometer with a rotating cylinder geometry generated via a uniaxial torque was used to study the viscosity and shear stress of the molten coal ash slag at different applied shear rates (0.34–34.00 s^{-1}), times (0–1.05×10^5 s), and temperatures (1400–1280°C) in an N_2 atmosphere. The change range of shear rate in our experiment is determined by referring to the data from literature and the coverage of their research range.[17,41] Figure 1a shows the high-temperature rheometer. The spindle was calibrated against Brookfield standard oil with nominal viscosities of 5.00, 30.00, 60.00, and100.00 Pa s at 25°C in the range of actual rotation rates and at high temperature with a standard reference material developed in the bureau communautaire de référence (BCR) program of the european union (EU); the viscosity measurement accuracy is to within ±10.00% of the full-scale range. This kind of rheometric measurements usually follow the standard analysis that is based on a key assumption: no-slip boundary conditions, as shown in Figure 1b.[42] However, in practice, one feature of concentric cylinder rheometer is the nonuniformity of the shear rate with the suspension sample, which apparently leads to a wall slip.[43] The wall slip phenomenon is produced by the relative velocity between the wall and the suspension at the wall, as shown in Figure 1c, which will possibly lead to a lower value for the measured viscosity compared with that of the true viscosity of suspensions.[44] One of the accepted ways to detect wall slip is to make the shear measurements of the same material for two different gap sizes (the distance between the inner spindle and the outer crucible) steady.[45] Figure 1d shows that the viscosity corresponding to the same temperature of the molten coal ash sample tested using different spindles is different at low temperatures. The observation illustrates that a wall slip was produced in our experiment. The measured deviation of the viscosity caused by the wall slip is approximately nearly 5.00%. The best

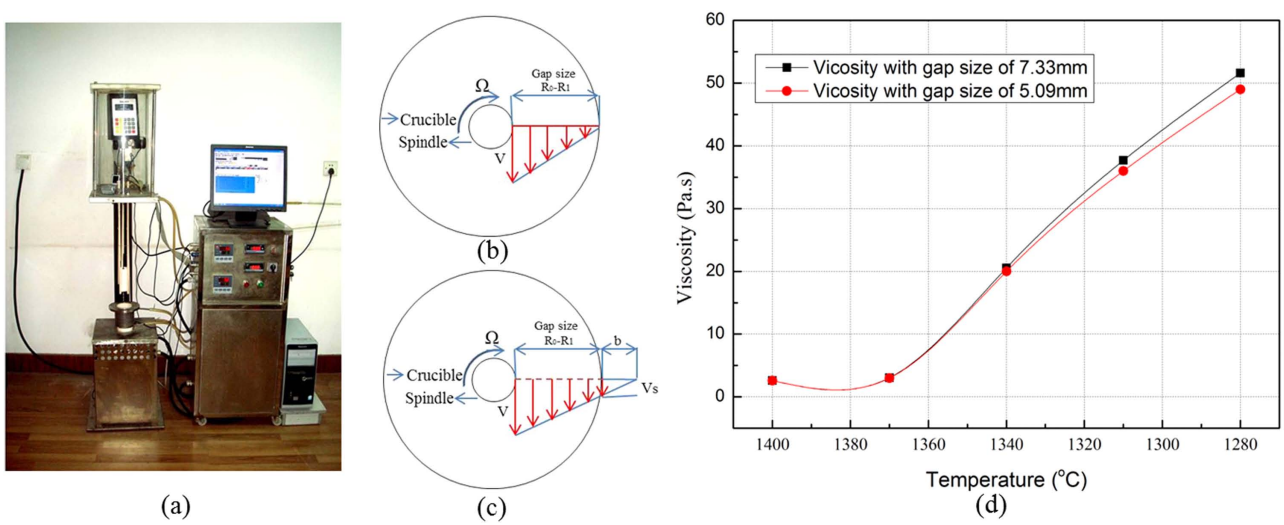

Figure 1. (a) High-temperature rheometer.

(b) Velocity profile diagram in cylindrical annulus without slip boundary condition. (c) Velocity profile diagram in cylindrical annulus with slip boundary condition. (d) Viscosity of the molten coal ash sample tested with different gap sizes at different temperatures. [Color figure can be viewed in the online issue, which is available at wileyonlinelibrary.com]

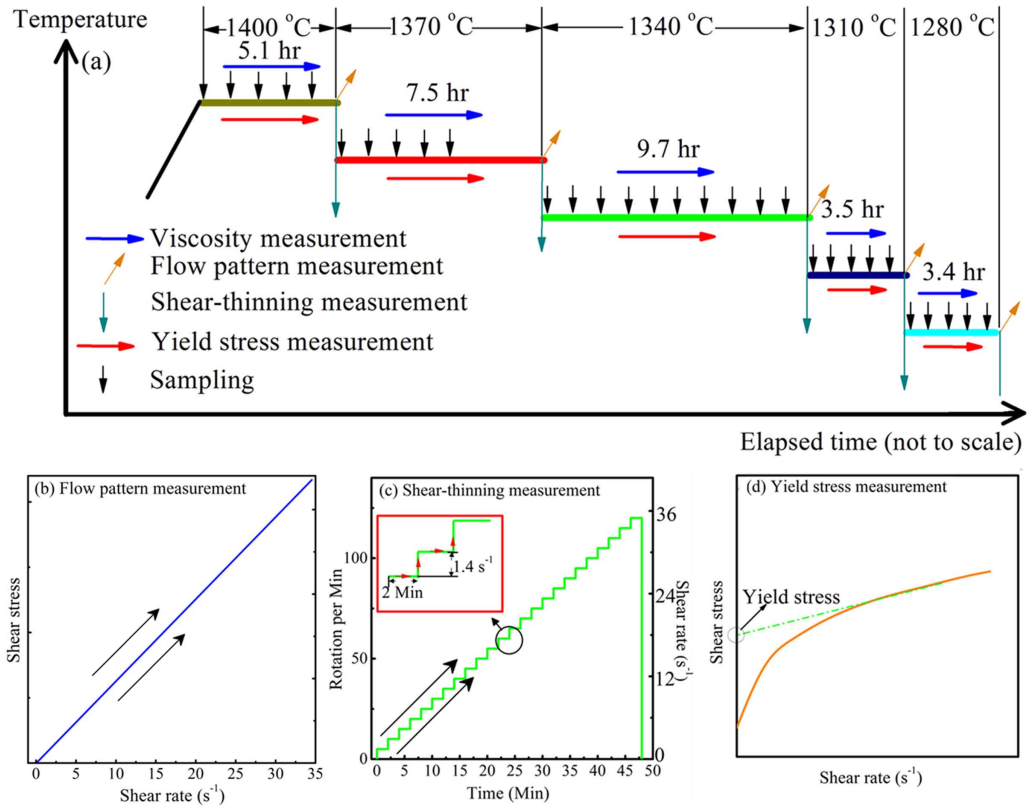

Figure 2. (a) Temperature-time schedule of the experiment.

The blue, dark cyan, red, and blank arrows indicate the viscosity measurement, the timing of the shear thinning measurement, the flow curve measurement, and sampling (wherein a few of the molten coal ash slag samples were directly transferred from high-temperature rheometer and quenched in liquid nitrogen, and subsequently transformed into polished thin sections for textural analysis), respectively. (b) Relationship of the shear stress and shear rate in the flow pattern measurement. (c) Relationship of the shear rate and the time of shear-thinning measurement. (d) The yield stress measurement method. [Color figure can be viewed in the online issue, which is available at wileyonlinelibrary.com]

methods in dealing with the wall slip in suspension are to use the vane geometry spindle to replace cylindrical spindle or a mathematical treatment for wall slip correction.[46,47] However, it is difficult to create the vane geometry shape of the corundum spindle due to the limitation of ultrahigh temperature. Moreover, the limitation deters the measurement of the necessary parameters (e.g., shear rate at a constant shear stress) required to calculate the effect of the wall slip on viscosity when using the mathematical models.[48,49] Therefore, the viscosity obtained in our experiment may be dependent on the size of the spindle and the crucible because of the nonuniform shear rate in these experiments. The detail information on this apparatus was previously reported.[28]

Figure 2 shows the temperature-time schedule of the experiment. The experimental arrangement for this investigation combines three experimental procedures, given that the viscosity measurement and flow pattern measurement (which indicates the relationship between the shear stress and the shear rate) could not be performed simultaneously, and that the sampling procedure would affect the experimental results during the viscosity and flow pattern measurements.

Approximately 90 g of coal ash samples were placed into a corundum crucible and slowly heated to 1400°C. This temperature was maintained for 1 h to ensure that the starting material is completely melted. Subsequently, the viscosity was measured using the spindle with a gap size of 7.33 mm under the specific shear rate for $\sim 1.84 \times 10^4$ s (5.1 h). The sample was then quickly cooled by 30°C, and the temperature was maintained for another 2.74×10^4 s (7.5 h). The temperature of the molten coal ash slag was lowered by 30°C for the subsequent measurement step. This sequence of viscosity measurements and stepwise cooling was repeated until the temperature decreased to 1280°C (Figure 2a). The cooling rate during the transition between steps was 3°C s^{-1}. Approximately 1.21×10^4 s to 3.50×10^4 s residence time at each 30°C interval was allowed at each temperature to ensure that the molten coal ash slag reached the perfect thermal equilibrium. At temperatures below 1280°C, viscosity measurements could not be performed because the large number of crystals and the resulting high viscosity of molten coal ash slag made the rotation of the rod impossible. At the end of each viscosity measurement, flow pattern measurement and shear-thinning measurement were conducted, respectively. The detailed experimental steps for the flow pattern and shear-thinning measurements are shown in Figures 2b, c. For the flow pattern measurement, the shear rate increased from 1 rpm to a certain maximum value in 1 rpm increments. The torque response at each shear rate was recorded. After the flow pattern measurement, the shear-thinning measurement started at 5 rpm and took one data point per second, and then subsequently went on standby for 120 s. Consequently, speed increased by 5 rpm, and data collection was repeated until obtaining a certain maximum value. The viscosity response at each shear rate was recorded.

After the above rheological measurements, the molten coal ash sample was again heated to 1400°C for the yield

stress measurement. This temperature was maintained for 1 h to ensure that the starting material was completely molten and in the same condition as that of the viscosity measurement. The temperature-time schedule used in the yield stress measurement was similar to that of the viscosity measurement. The sequence of stepwise cooling, holding at a constant temperature, and cooling at a specific temperature rate are the same as that for the viscosity measurement. Owing to the difficulties of directly measuring yield stress, for all of the slag temperatures tested in our experiments, yield stress values have been obtained by extrapolation of the straight-line portion of the stress-shear rate curve to the intercept on the stress axis (Figure 2d). The yield stress measurement was conducted until the temperature went below 1280°C. At each temperature, the measurement was conducted by rotating the spindle at a low speed and measuring the torque acting on it. The rotational speed was then increased from the minimum value to some maximum value to a specific maximum value, and the torque response at each constant speed was recorded. Then, the yield stress values of the samples were determined from the ascending part of the flow curves.

After the yield stress measurement, the molten coal ash sample was again heated to 1400°C to observe the crystal behavior and evaluate the growth histories of the crystal population. The temperature-time schedule in the sampling process was the same as that in the viscosity measurement. About 2 g of molten coal ash slag samples were directly and rapidly collected from the high-temperature rheometer approximately every 3600 s at 1400 and 1370°C, and 1800 s at 1340, 1310, and 1280°C (Figure 2a, black arrows). The samples were then rapidly quenched in liquid nitrogen.

Textual analysis

Some experimental work suggests that the viscosity of the molten coal ash slag significantly changes during progressive crystallization.[50] Therefore, general knowledge of the effect of changes in crystallization on the evolution of the rheological properties of molten coal ash slag is a major interest area.

The quantitative measurement of the textual characteristics of the crystallized particles in the quenched molten coal ash slag was performed on the basis of the binary images obtained through an optical microscope (LV100POL, Linkam Scientific Instruments) with a reflected light source. A series of digital microphotographs of the crystals was taken, stored in a computer, and analyzed to determine the crystal average length, crystal average number density, and crystal volume fraction of the two-dimensional (2-D) intersection using the NIH Image program (freeware from National Institute of Health http://rsb.info.nih.gov/nih-image/index.html). The micrographs of the molten coal ash slag samples taken and quenched according to our experimental temperature-schedule are shown in Figure 3.

One challenging aspect of CSD analysis is that the fundamental variable, population density, is a volumetric parameter that cannot be directly measured on the sections of the cooling sample. Therefore, the 2-D intersection data must be converted to 3-D CSDs. This solution is not simple, unless the crystals are assumed to be spherical in shape. Many investigators have used stereological transformations from 2-D to 3-D to obtain the volume-normalized population densities.[51,52] In the current study, the CSD correction method proposed by Higgins[53] was used for the 3-D calculation. This method is a modification of that of Saltykov,[54] which "unfolds" the intersection data to yield the true CSDs. Once the crystal size data were obtained via image analysis, they were sorted into class intervals and then converted to microns at each given magnification. Logarithmic length intervals were used so that each bin is $10^{0.1}$ times the size of the previous bin. This bin width ensures that an adequate number of crystals are in each bin. Each bin contains at least one crystal, and no gaps with empty bins exist. The volume of each crystal was calculated by taking the measured projected area of the crystals that is equivalent to the area of an equivalent sphere; the equivalent spherical diameter for each crystal was then used to calculate the volume of each crystal, following the method of Bindeman.[55]

The Equilib module in FactSage 6.3 was used to conduct thermodynamic equilibrium modeling of the liquid temperature of the coal ash sample, composition of the mineral phase, and viscosity of the remaining homogenous phase under air condition at a pressure of 1 atm at different temperatures based on Gibbs energy minimization. Phase formation data for these oxides and their combinations were selected from the FToxide database. The calculation method of FactSage is based on Gibbs's energy minimization for each of the samples at a given temperature and composition range. The database used includes solid pure components and polynomial solid solutions.

Thermodynamic modeling

In our work, the thermodynamic properties of the molten coal ash slag have been calculated from the (SiO_2–Al_2O_3–CaO–Fe_2O_3–MgO–TiO_2–Na_2O–K_2O) system using the FactSage software package.[56] The liquid temperature of the sample, composition of the mineral phase, and viscosity of the remaining homogenous phase were evaluated under air condition at a pressure of 1 atm at different temperatures based on the oxide composition of the sample. Further information about thermodynamic modeling (i.e., database and phase selection) is provided in Supporting Information.

Results and discussion

Rheological evolution

Viscosity. A series of rheometric measurements was performed on the high-temperature rheometer. Figure 4 shows the experimental results of the successive viscosity measurements of the molten coal ash slag at 1400–1280°C. At the highest temperature in our experiment (1400°C), the obtained viscosity profile (Figure 4a) reveals viscosity values that are mainly constant with time. When the temperature is decreased from 1400 to 1370°C, a slight viscosity increase at the initial stage of cooling is observed until a certain value is reached in a short time and then remains unchanged. This result indicates that this sample can rapidly reach the steady condition and that the effect of the changes in temperature and time on the viscosity when temperature is decreased from 1400 to 1370°C is slight. However, when the temperature is decreased from 1370 to 1340°C, the viscosity markedly changes during the total measurement, increasing from 3.05 to 23.55 Pa s. This result indicates that at 1340°C, several complex changes occur in the sample, including the chemical reaction of the homogenous liquid, nucleation, and crystallization in the molten coal ash slag before the viscosity value constant is reached. Finally, when the temperature

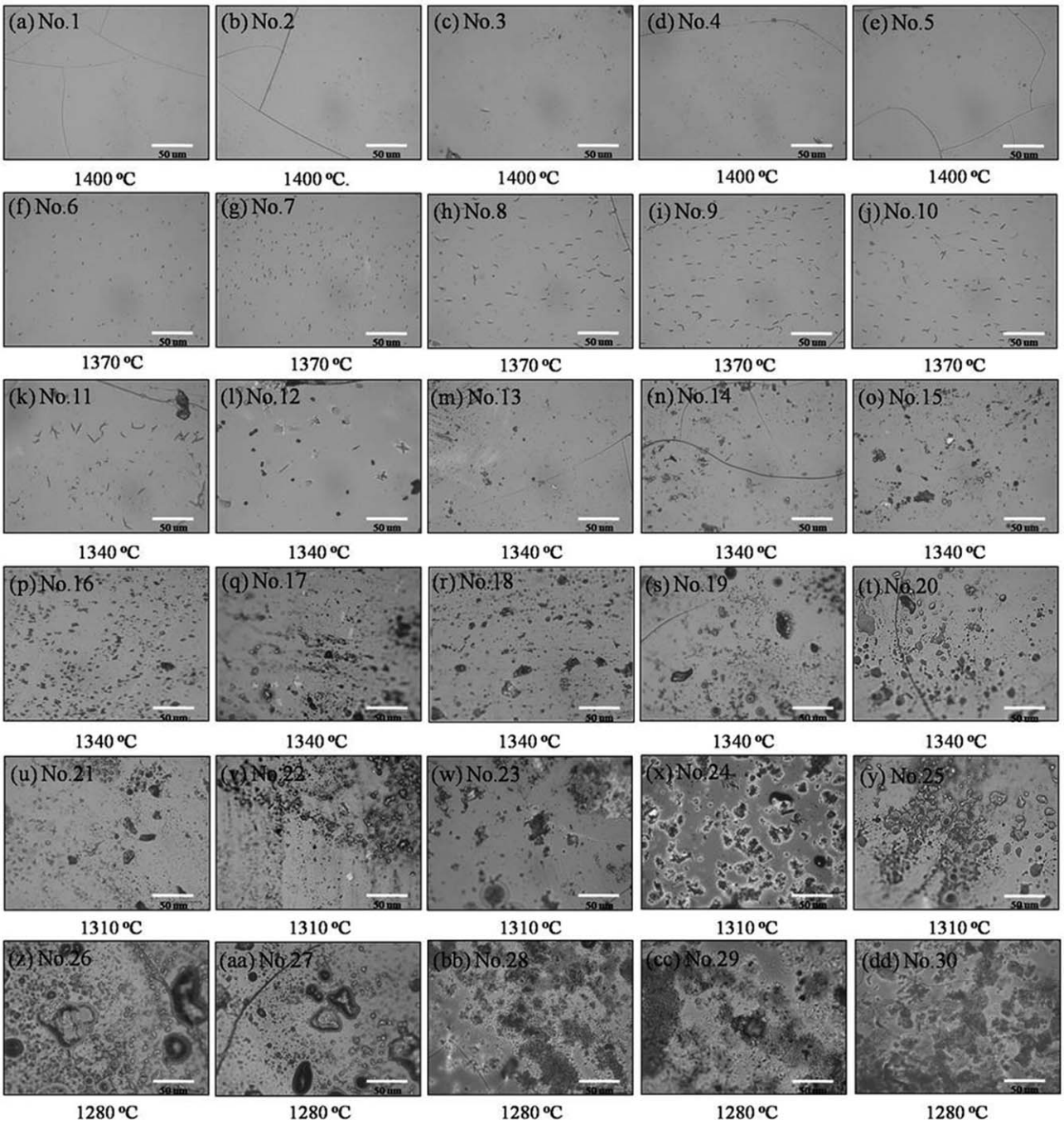

Figure 3. Transition of the surface morphology of the molten coal ash slag samples taken and quenched in our experiment.

is decreased to 1310 and 1280°C, the viscosities continuously increase until they stabilize to a constant value.

Figure 4b shows the change rate of viscosity with time ($d\eta/dt$) during the viscosity measurements, which provides an approximation of the time at which the sample reaches the steady condition. These observations in Figure 4b suggest that during the decrease in temperature, differences in the effect of temperature on viscosity corresponding to different temperatures are observed. The nearer the temperature corresponding to the test viscosity is to the highest temperature, 1400°C, the less the effect of temperature and time on viscosity. For example, the change trend of the $d\eta/dt$ gradient of the sample at lower temperatures (from 1340 to 1280°C) is clearly more pronounced than that at higher temperatures (1370 and 1400°C), suggesting a relatively stronger contribution of crystals at 1340, 1310, and 1280°C up to the melt behavior because of the increase in the crystal constant with decreasing temperature. These findings play a pivotal role in assessing the flow mechanism, particularly the role of time and temperature in the documented case.

Figure 5a shows the viscosity-temperature curves of the molten coal ash slag at the initial cooling stage (blue curve, initial) and on reaching thermodynamic equilibrium (red curve, final). When the temperature is in the 1400–1370°C range, the two viscosity curves for the initial and final conditions almost coincide. However, when the temperature is

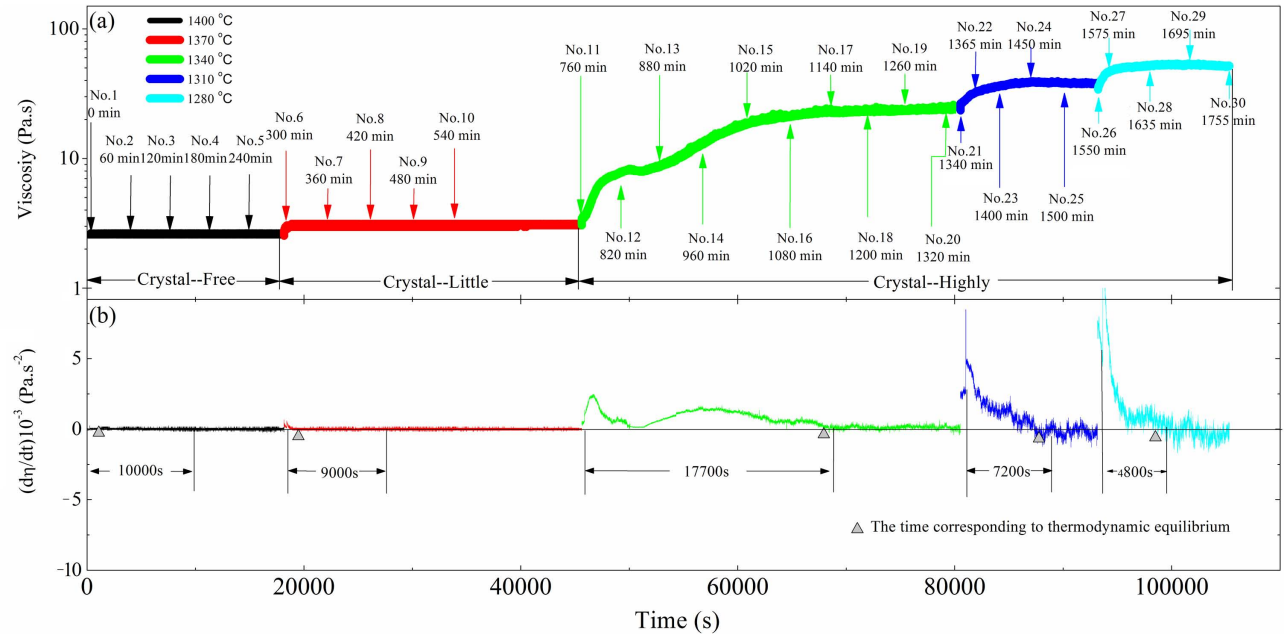

Figure 4. Experimental results of the successive viscosity measurements of the molten coal ash slag at 1400, 1370, 1340, 1310, and 1280°C.

(a) The apparent viscosity profile shows the successive changes in the viscosity with each time increment at each temperature. The black arrows show the samples taken in our experiments. The three sections are grouped according to the crystal concentrations, as follows: crystal free, crystal little, and crystal high. (b) The rate of change in viscosity is plotted vs. time. [Color figure can be viewed in the online issue, which is available at wileyonlinelibrary.com]

lower than 1370°C, the red viscosity curve under the finial condition is clearly higher than the blue one. This result is due to the formation of crystalline particles and the gradual increase in their number in the molten coal ash slag with deceasing temperature when the temperature is lower than 1370°C, which results in an increase in viscosity (Figure 5a). The value of the relative increase in the viscosity at the final and initial stages is compared, and is defined as

$$\Delta\eta_s = \frac{\eta_{s,final} - \eta_{s,initial}}{\eta_{s,initial}} \times 100\% \quad (4)$$

where $\Delta\eta_s$ is the relative increase in the viscosity value, $\eta_{s,final}$ is the viscosity at the final condition when the sample reaches the steady condition, and $\eta_{s,initial}$ is the viscosity at the initial cooling condition. Figure 5b shows that when the

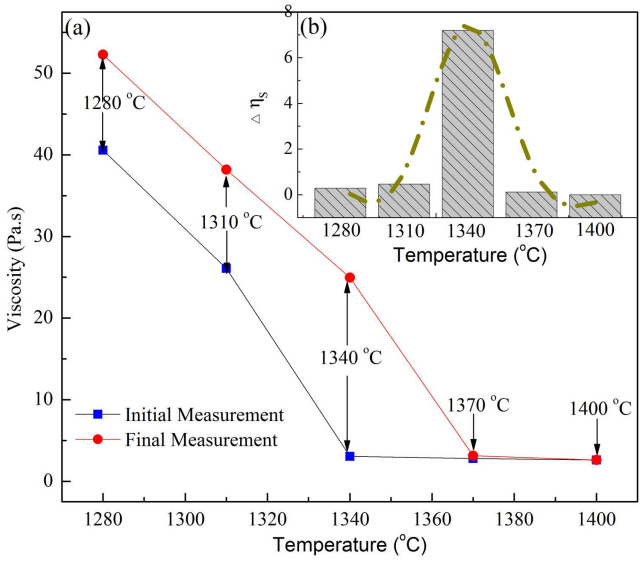

Figure 5. Flow properties of the molten coal ash slag.

(a) Initial and final viscosity-temperature plots of the molten coal ash slag. (b) Comparison of the relative increase in the viscosity at different temperatures. [Color figure can be viewed in the online issue, which is available at wileyonlinelibrary.com]

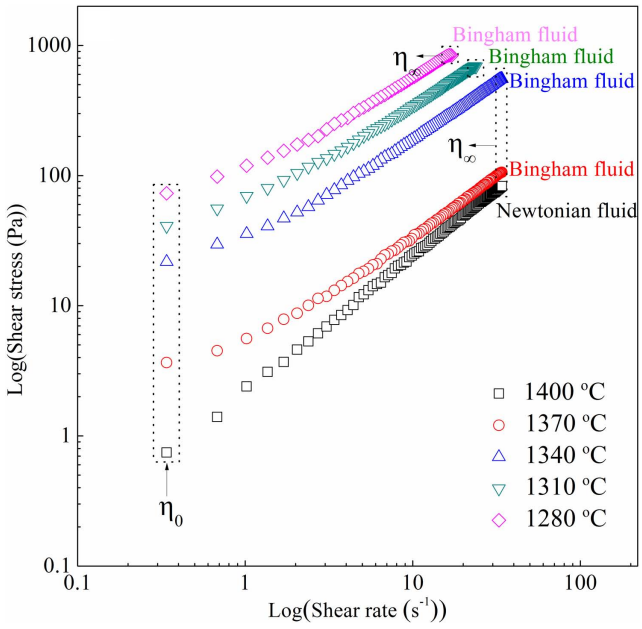

Figure 6. Shear stress-shear rate curves for the three simple rheological laws approximating the molten coal ash slag behavior.

[Color figure can be viewed in the online issue, which is available at wileyonlinelibrary.com]

Table 2. Constitutive Equations of the Molten Coal Ash Slag at Different Temperatures

Temperature (°C)	Model	Constitutive Equations	Correlation Coefficient, R^2	Standard Deviation, SD[a]
1400	Newtonian	$\tau_w = 2.39\dot{\gamma}$	0.99	0.34
1370	Bingham	$\tau_w = 3.06 + 3.71\dot{\gamma}$	0.99	0.42
1340	Bingham	$\tau_w = 28.54 + 15.89\dot{\gamma}$	0.99	4.53
1310	Bingham	$\tau_w = 54.28 + 27.91\dot{\gamma}$	0.99	6.45
1280	Bingham	$\tau_w = 83.36 + 47.62\dot{\gamma}$	0.99	9.74

[a]The standard deviation (SD) indicates the degree of variation in relation to the average mean.

sample begins to cool, the relative increase in the viscosity values at 1400 and 1370°C is almost equal to zero. When the temperature is decreased to 1340°C, the relative increase in the viscosity value clearly increases and reaches a maximum value, then decreases before increasing once more, indicating that the viscosity of the molten coal ash slag sample is most sensitive to change of temperature during attainment of the steady condition at 1340°C.

Flow pattern. A 2-D variation diagram of the relationship between the shear stress and shear rate of molten coal ash slag under different temperatures is constructed in Figure 6. The diagram provides a visualization of the behavior transition of molten coal ash slag from Newtonian to non-Newtonian with the decrease in temperature from 1400 to 1280°C. Providing an extra definition of the rheology of molten coal ash slag at a high temperature is technically difficult; thus, some well-known laws were used to give a reasonable approximation to describe the rheological characteristics of the molten coal ash slag under different temperatures and according to the characteristic shape of the flow curves.

1. Newtonian model[57]

$$\tau_{\mathrm{w}} = \eta_N \cdot \dot{\gamma} \tag{5}$$

2. Bingham model[58]

$$\tau_{\mathrm{w}} = \tau_{\mathrm{Y}} + \eta_B \cdot \dot{\gamma} \tag{6}$$

where τ_{w} is the shear stress, τ_{Y} is the yield stress (or internal cohesion), $\dot{\gamma}$ is the shear rate, and η_N and η_B are the coefficients of the Newtonian model and Bingham model, respectively. For any flow pattern at any shear rate, the ratio $(\tau_w/\dot{\gamma})$ is the apparent viscosity, η_s, which is simply called viscosity according to Nzihou et al.[59]

$$\eta_s = \tau_w/\dot{\gamma} \tag{7}$$

The flow curves of the molten coal ash slag as shown in Figure 6 are modeled by constitutive equations of the Newtonian model and Bingham model (Eqs. 5 and 6). The constitutive equations that describe the flow behaviors of the molten coal ash slag under different temperature are given in Table 2. As shown in Table 2, the relationship between the shear stress and shear rate of the sample is modeled by a straight line through the origin when the temperature is 1400°C, which is indicative of an almost Newtonian behavior of the sample at this temperature. As the temperature is decreased, the flow curves of the sample are changed. The molten coal ash slag becomes a Bingham fluid when the temperature is lower than 1400°C, in which the relationship between the stress and shear rate of the sample remains linear but its intercept is above zero, thereby indicating the presence of yield stress.

Shear thinning. The viscosity of the molten coal ash slag is affected by the viscosity of the continuous phase and the solid-phase concentration, as well as by the shear stress or the shear rate. Figure 7a shows the shear rate dependence of the viscosity at various temperatures. Vertical points in Figure 7a indicate actual variations of viscosity values of coal ash slag at the same shear rate for a certain period (120 s in our experiment), and the plots in each temperature are the average viscosity values at the same shear rate for a certain period. At 1400°C, hardly any crystals are present in the molten coal ash slag (Figure 3e), and the viscosity is largely constant regardless of the rotation rate, indicating that the molten coal ash slag at this temperature behaves like a Newtonian fluid. When the temperature is decreased to 1370°C, the amount of crystals increases to 4.71 vol % (Figure 3j), and the viscosity slightly decreases with increasing shear rate. However, the variations in the apparent viscosities become increasingly sensitive to the shear rate when the temperature is continually decreased because of the strongly non-Newtonian behavior of crystal-bearing molten coal ash slag. This behavior, known as "shear-thinning," is common with silicate melts, particulates suspensions, including colloidal suspensions and attractive emulsions.[60,61] Meanwhile, the change rate of viscosity with the shear rate at the shear-thinning measurement is defined as

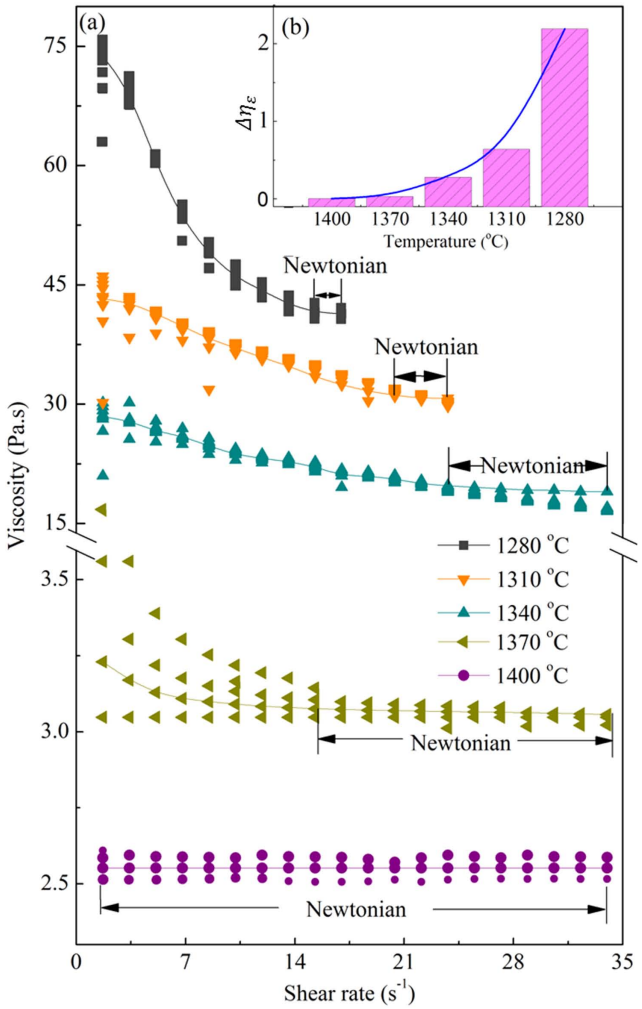

Figure 7. Shear-thinning behavior of the molten coal ash slag.

(a) Relationship between the measured viscosity and shear rate at different temperatures. (b) Comparison of the change rate of viscosity at increasing shear rate under different temperatures. [Color figure can be viewed in the online issue, which is available at wileyonlinelibrary.com]

$$\Delta\eta_{\varepsilon} = \frac{\eta_{\varepsilon,\text{initial}} - \eta_{\varepsilon,\text{final}}}{\Delta\dot{\gamma}} \tag{8}$$

where $\Delta\eta_{\varepsilon}$ is the change rate of viscosity with respect to shear rate; $\eta_{\varepsilon,\text{initial}}$ and $\eta_{\varepsilon,\text{final}}$ are the viscosity values at the initial and final condition in the shear-thinning measurement, respectively; and $\Delta\dot{\gamma}$ is the increase in the shear rate from the initial to the finial conditions. As the shear rate is increased, the change rate of viscosity with the shear rate is slightly increased compared with that at 1400°C, and dramatically increases as the temperature is decreased to below 1370°C (Figure 7b). These results indicate that the shear-thinning behavior becomes even more distinct with decreasing temperature mainly because of the formation of a number of crystalline particles in the molten coal ash slag at temperatures lower than 1370°C. The change rate of the viscosity with the shear rate reaches its maximum value at 1280°C.

Generally, two regions in the curves of shear-thinning behaviors indicate that the viscosity is constant at very low and high-shear rates. These two extremes correspond to the first and second Newtonian regions (Supporting Information, Figure S1).[62] However, the curves in our experiment did not exhibit the first Newtonian region due to the limitation of the lowest-shear rate. The curves exhibited the second Newtonian region because of the change in geometrical redistributions of the suspended particles.[63]

Yield stress. Figure 8 shows the process of onset and yield stress development of molten coal ash slags as well as the relationship between yield stress and crystal volume fraction in the molten coal ash slag. The evolution of the yield stress vs. time at 1400–1280°C is shown in Figure 8a. At 1400°C, the yield stress is essentially equal to zero regardless of the time because of the free crystals in the molten coal ash slag at this temperature. When the temperature is decreased to 1370°C, yield stress appears and increases, and the final yield stress becomes higher than the initial ones because of the slight increase in the crystal content of the molten coal ash slag with increasing time. Furthermore, the relative value of the yield stress clearly increases and reaches its highest value at 1370°C (Figure 8b). The definition of the relative increase in the yield stress is defined as

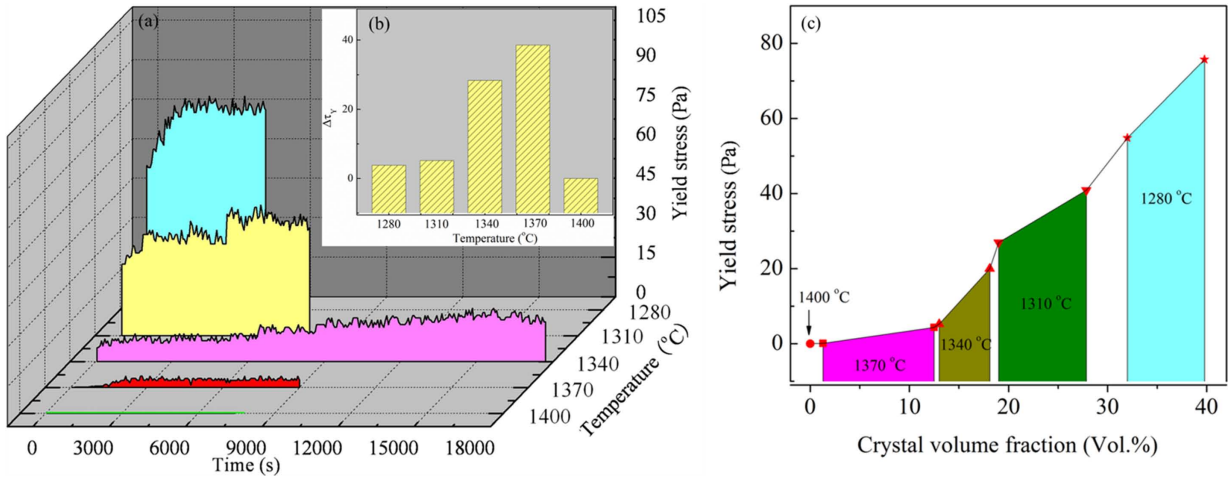

Figure 8. Yield stress evolution in the molten coal ash slag.

(a) The yield stress in the molten coal ash slag as a function of time at different temperatures. (b) Relative increase in the yield stress from the final to the initial values during the cooling process. (c) The yield stress as a function of the volume fraction of the crystal in the molten coal ash slag. [Color figure can be viewed in the online issue, which is available at wileyonlinelibrary.com]

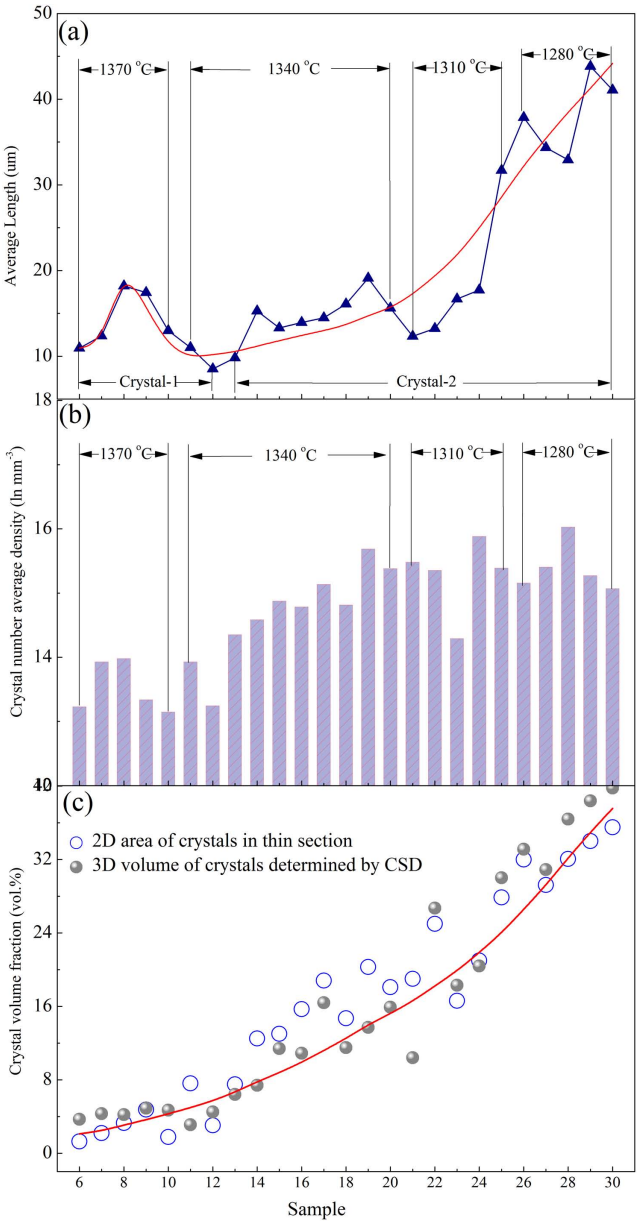

Figure 9. Textural variations in crystal-1 and crystal-2 in the molten coal ash slag samples at different temperatures.

(a) Crystal average length. (b) Crystal average number density. (c) Crystal volume fraction. [Color figure can be viewed in the online issue, which is available at wileyonlinelibrary.com]

$$\Delta\tau_Y = \frac{\tau_{Y,\text{final}} - \tau_{Y,\text{initial}}}{\tau_{Y,\text{initial}}} \times 100\% \quad (9)$$

where $\Delta\tau_Y$ is the relative increase in yield stress, $\tau_{Y,\text{final}}$ is the yield stress at the final condition when the sample reaches the thermodynamic equilibrium in the yield stress measurement, and $\tau_{Y,\text{initial}}$ is the yield stress at the initial cooling condition in the yield stress measurement. Finally, at 1310°C and 1280°C, the yield stress of the molten coal ash slag suspension appears to remain constant when the solid concentration reaches a finite value with increasing time.

The textural variations in the crystal average length, crystal average number density, and crystal volume fraction as a function of time at different temperatures are shown in Figure 9 to shed light on the effects of crystal volume fraction on yield stress. Figures 9a, b show that the average length and crystal average number density of crystal-1 in the initial cooling stage at 1370°C initially increased and then reaches the maximum values, before again decreasing as time is increased. In contrast, the average length of crystal-2 increases with increasing time and decreasing temperature in general, and the crystal average number density slightly increases with increasing time at 1340°C as a whole. In addition, the crystal volume fraction determined by the thin section (2-D) and CSD (3-D) increase with increasing time and decreasing temperature, as shown in Figure 9c.

Figure 8c also shows the relationship between yield stress and crystal volume fraction in the molten coal ash slag tested in our experiment. It can be seen that the onset of yield stress can be estimated to occur during the process of achieving the steady condition at an initial temperature of 1370°C, which corresponds to crystal volume fractions between 0 and 4.71 vol %. When the temperature is decreased from 1370 to 1340°C, the yield stress is significantly increased because the proportion of solid phase in the slag rapidly increases the crystal volume fractions from 4.70 to 18.13 vol %, and the possible development of a 3-D framework of crystals inhibits flow movement at low stresses.[64] Finally, at 1310 and 1280°C, the yield stress of molten coal ash slag suspension rapidly increases with increasing crystal volume fraction. This phenomenon indicates that crystallization is one of the main factors that affect the change in the yield stress.

Crystallization response

Texture. Figure 3 shows micrographs of the molten coal ash slag samples (Nos.1–30) taken and quenched according to our experimental temperature schedule. All images show an increase in crystal volume fraction with decreasing temperature and increasing time at constant temperature. In samples with lower crystal volume fraction, the spatial distribution of the crystals is heterogeneous, with microphysical aggregates intergrown among the crystal particles and separated by larger pockets of glass. However, in highly crystalline samples, the particles form a spatially homogeneous crystalline texture, usually with intricate intergrowths of crystal particles that resemble crystal habits typical of high-cooling rates.[65]

Figures 3a–e show that sample Nos. 1–5 taken at 1400°C are poorly crystalline. As the temperature is decreased to 1370°C, small amount of crystal particles is generated in the Nos. 6–10 molten coal ash slag sample as shown in Figures 3f–j. According to the estimation of FactSage, a single-crystal phase [$Ca(Al,Fe)_{12}O_{19}$] possibly exists above 1370°C. Therefore, the crystals in the molten coal ash slag samples Nos. 6–10 are defined as crystal-1 in our experiment. When the temperature is decreased to 1340°C, the crystal shape in Figure 3k is similar to those of crystals generated at 1370°C at the initial stage; thus, the crystals in Figure 3k are also defined as crystal-1. As time is increased at this temperature, crystal-1 disappears and a new crystal phase, possibly mullite, is generated, as predicted by FactSage; these crystals are defined as crystal-2. The free-energy barrier associated with the formation of an interface separating the new and old phase is lowered due to the disappearance of the original crystal phase (crystal-1) and the generation, nucleation, and

growth of a new crystal phase (crystal-2). This phenomenon significantly accelerates the nucleation and growth of the new crystal phase at 1340°C. When the temperature is decrease to 1310 and 1280°C, cooling and crystallization during the flow generate abundant crystal particles in the molten coal ash slag and form a spatially pseudohomogeneous crystalline texture, resulting in high-viscosity and high-yield stress.

Crystal-size distribution. To establish the crystal population balance in the molten coal ash slag, the number of crystals per size and per unit volume of the slag solution must be considered as a function of the crystal size. The population density (n_i) of a crystal phase i ($i = 1$, the crystal phase is crystal-1; $i = 2$, the crystal phase is crystal-2) is defined as the number of crystals in any size range divided by the size interval, as follows

$$n_i(L) = \frac{\Delta N_i}{\Delta L_i} (i = 1, 2) \tag{10}$$

where N_i is the total number of crystal phase i (1 and 2) in the molten coal ash slag of a size less than L_i, and L_i is some characteristic crystal size. Accordingly,

$$N_i(L) = \int_0^{L_i^*} n_i(L_i) dL_i (i = 1, 2) \tag{11}$$

where L_i^* is upper limit of the integration. A steady-state population balance of crystals growing into and out of a specific size range L_i, while physically circulated into and out of the system at the same time is described by

$$\frac{d(G_i n_i)}{d(L_i)} = -\frac{n_i}{\tau_i} (i = 1, 2) \tag{12}$$

where G_i is the growth rate of crystal phase i, and τ_i is the residence time of crystal phase i. If G_i is independent of L_i,[66] Eq. 12 may be integrated to give

$$n_i = n_i^0 e^{(-(L_i - L_0)/G_i \tau_i)} (i = 1, 2) \tag{13}$$

L_0 is the initial nucleus size with a value of approximately zero. The quantity n_i^0 is a constant of the integration and represents the population density of the nucleus-size crystals (n_i as $L_i \rightarrow 0$). When L_0 is equal to zero, Eq. 13 can also be expressed in the following form

$$In(n_i) = In\left(n_i^0\right) - L_i/(G_i \tau_i) (i = 1, 2) \tag{14}$$

The CSD method indicates that under certain circumstances (i.e., steady-state conditions, size-independent crystal growth) the natural logarithm of the population density of crystals (i.e., the number of crystal within a specified size interval per unit volume of the silicate and divided by the width of the specified interval) linearly varies with and is inversely proportional to the crystal length. In other words, a plot of $In(n_i)$vs.L_i for a steady-state system will be a straight line with a slope equal to 1 / (growth rate × residence time) ($1/G_i \times \tau_i$), and an intercept equal to the nucleation density (n_i^0). The plot of the crystal length vs. the population density is generally called a CSD plot. However, in our experiment, most of the CSD plots are not linear (not exponentially distributed) at the upper ranges of L_i (Figure 10) because the samples were taken in nonsteady-state conditions. Therefore, the maximum length (L_i^*), which corresponds to the vertical broken line in Figure 10, is defined as the intercept of the exponential law on the size axis corresponding to the highest value of the correlation coefficient (R^2 exponential law), as obtained using a regression line. The crystal population density calculated according to the exponential law up to L_i^* is similar to the total crystal population density up to the maximum size because the crystal population density is mainly controlled by crystals of smaller sizes. Consequently, the total crystal population density is regarded as the integration of the straight CSD line from 0 to the upper limit of the exponential law.

The raw size data of crystal-1 in sample Nos. 6–11 and crystal-2 in samples Nos. 12–30 in the molten coal ash slag were stereologically corrected and plotted in Figure 10, which shows the CSD in these 25 samples. The absolute value of the slope ($1/G_i \tau_i$) and intercept (n_i^0) in the CSD curves of these samples can be obtained from Figure 10. If either the residence times are known, the growth rate may be determined. The broken lines indicate the limit of the exponential as determined by a survey of the correlation coefficient (R^2, exponential) for the regression lines.

The CSDs of crystal-1 are individually shown in Figures 10a–f and are compiled in Figures 11a, b, which shows that the crystal-1 CSDs tend to have a small number of crystals. In Figures 11a, b, the crystal-1 CSDs exhibit a concave-down shape, indicating that small crystals are deficient compared with the linear CSDs observed in more mafic systems. The concave-down log-normal CSDs and decease in the population density may be due to textural coarsening, also known as Ostwald ripening, and textural maturation (Figure 11e).[34] Crystal-1 disappears as the temperature is decreased, and the other main crystal phase, crystal-2, begins to form. The CSDs of crystal-2 are individually shown in Figures 10g–y and are compiled at 1340, 1310, and 1280°C in Figures 11b–d, respectively. The CSDs of samples Nos. 13–20 at 1340°C show similar change trends and present upward curves due to the accumulation of crystals of different sizes (Figure 11f).[35] When the temperature is decreased to 1310°C, the CSDs of crystal-2 in sample Nos. 21–25 become irregular, with most exhibiting a sudden two-fold decrease because of the fine destruction and loss of the largest crystals (Figure 11j).[34] The population density in the CSDs of crystal-2 in sample Nos. 26–30 steeply descends to minus infinity from the left of the maximum, as shown in Figure 11d. The sudden change is possibly caused by the aggregation of small crystals to form larger crystals (Figure 11h).[34]

Nucleation and growth rates. To obtain information on original conditions of crystal nucleation and growth of molten coal ash slag, it is important to verify that the slope of a CSD plot. The population density of the crystal phase i, $In(n_i)$, is linearly correlated to crystal size L_i. When L_i is lower thanL_i^*, as previously shown by the empirical evidence in CSDs curves of molten coal ash slag samples. Therefore, the nucleation and growth rate can be obtained using the CSD method. So far, the growth rate (G_i), nucleation density (n_i^0), residence time (τ_i), and crystal rate (L_i) have been expressed in Eqs. 10–14. From Eq. 10, the nucleation density can be defined as

$$n_i^0 = \left.\frac{dN_i}{dL_i}\right|_{L_i = 0} (i = 1, 2) \tag{15}$$

However, the nucleation rate of the crystal phase i (J_i) is defined as

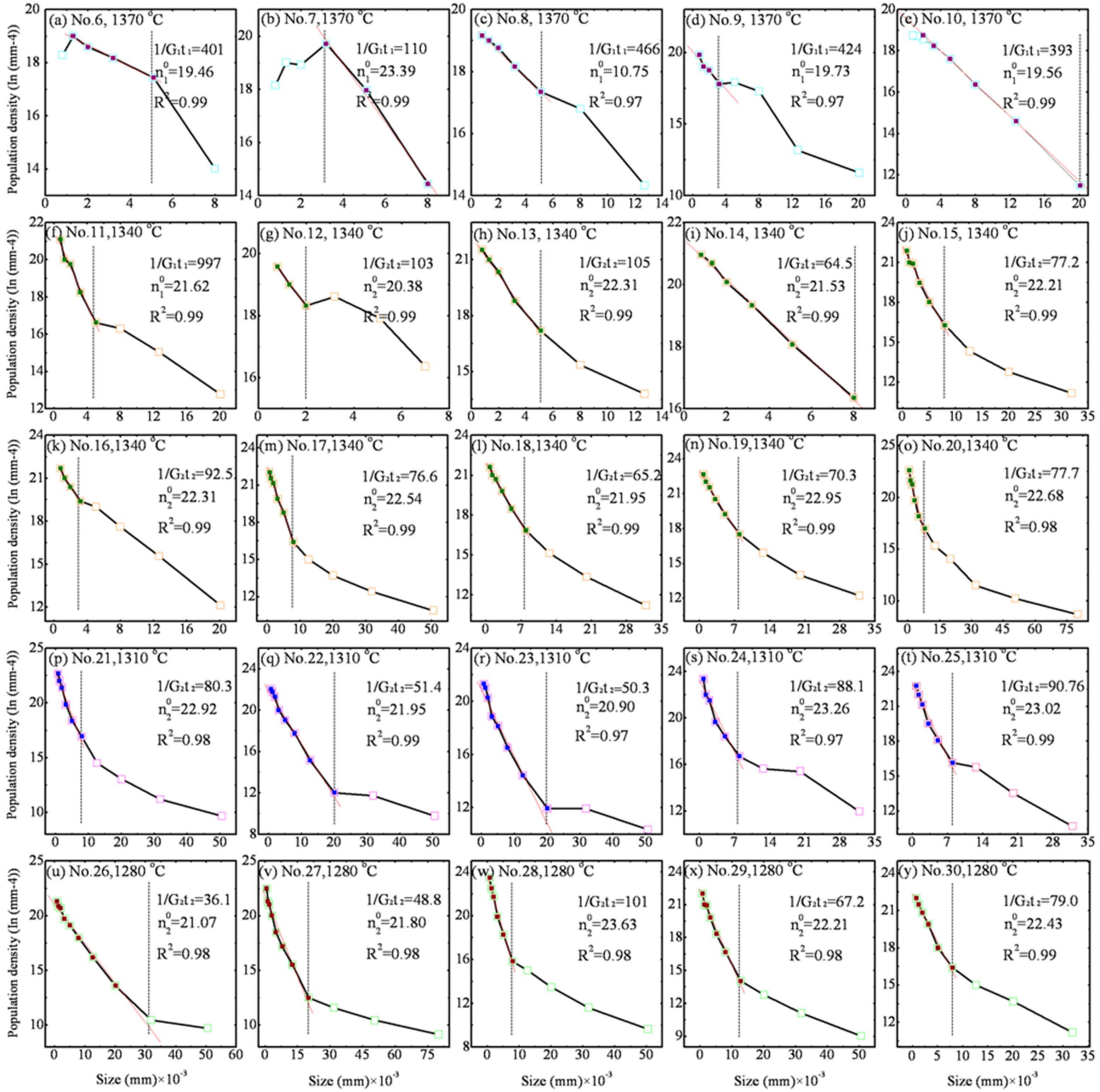

Figure 10. Graphs depicting the variations in the CSDs of crystal-1(Nos. 6–11) and crystal-2 (Nos. 12–30) from 25 molten coal ash slag samples.

The dotted line indicates the limit of the exponential though a survey of the correlation coefficient (R^2: exponential) for the regression lines. [Color figure can be viewed in the online issue, which is available at wileyonlinelibrary.com]

$$J_i = \left.\frac{dN_i}{dL_i}\right|_{L=0} \times \frac{dL_i}{d\tau_i} = n_i^0 \times G_i (i = 1, 2) \tag{16}$$

That is, the nucleation rate (J_i) is simply the product of the nucleation density (n_i^0) and the growth rate (G_i). Thus, a linear crystal size plot contains measurable parameters that can be directly related to the crystal nucleation rates, growth rates, and residence times.

When the slope, CSD curve intercept, and residence times are known, the growth rate can be determined by the intercept of the CSDs plot and then nucleation rate can be calculated by the absolute value of the CSDs plot slope. Figure 12 shows the nucleation and growth rates of crystal-1 and crystal-2, respectively, in the molten coal ash slag, as determined using the CSD plots. The change trends of the nucleation rates of crystal-1 and crystal-2 with increasing time are similar with that of the growth rate, indicating that the crystal growth is continuous throughout the crystallization interval. Both the crystal nucleation rate and the growth rate of crystal-1 initially increase, then reach the highest values and again decrease with increasing time. However, for crystal-2, the change rates of crystal nucleation and growth display wave curves, and the trend decreases with increasing time as a whole.

Rheology and crystallization

A number of studies have been devoted to the prediction of the viscosity of liquidus with solid suspensions; however,

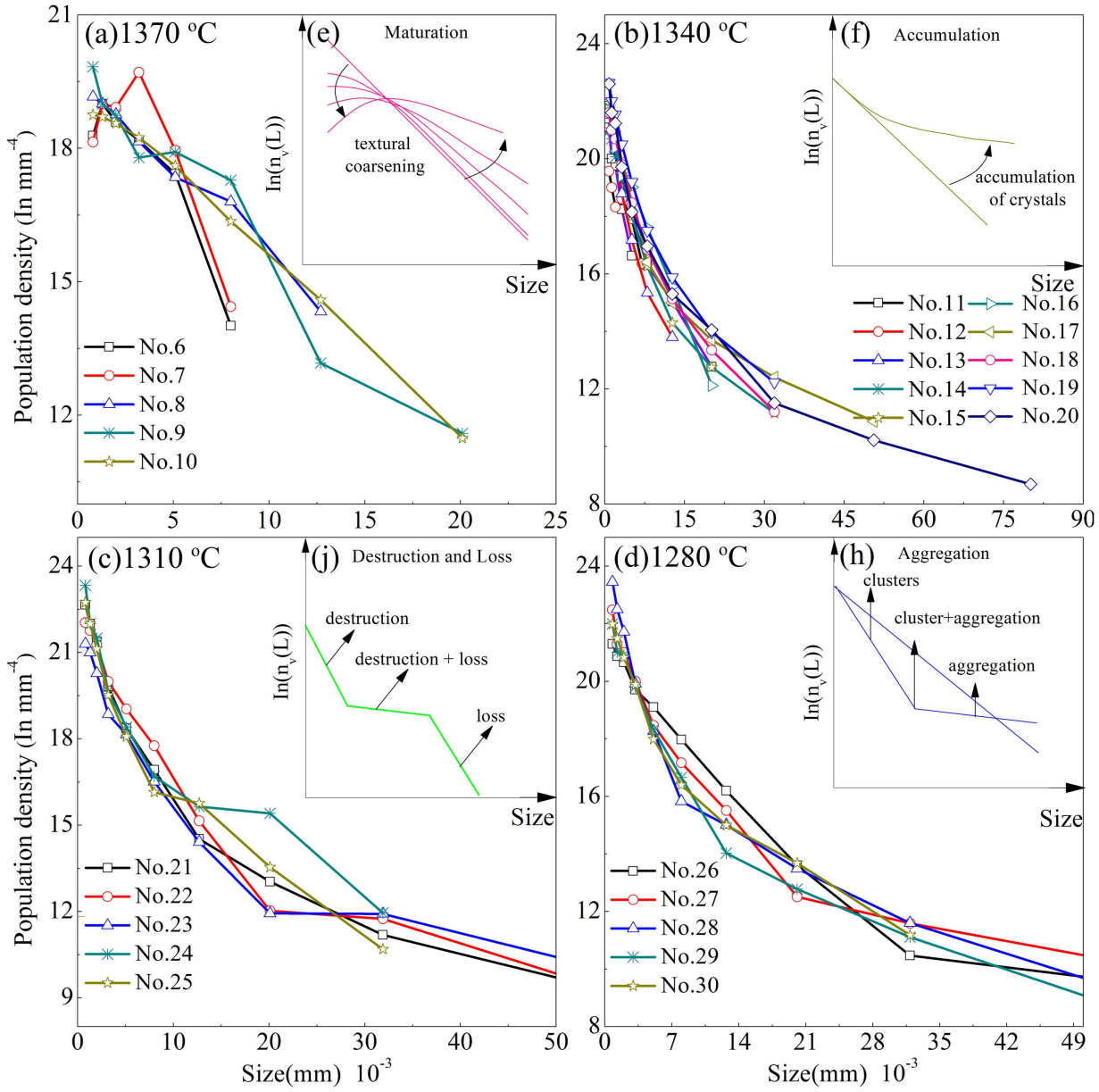

Figure 11. Compilations of CSDs: (a and b) crystal-1 in sample Nos. 6–11, and (b–d) crystal-2 in sample Nos. 12–30 in the molten coal ash slag samples at 1370, 1340, 1310, and 1280°C.

(e–h) Some dynamic processes that can affect the shape of the CSD. [Color figure can be viewed in the online issue, which is available at wileyonlinelibrary.com]

no rigorous theory, even for the simplest case of rigid spherical inclusions embedded in an incompressible Newtonian melt, has been proposed so far. For example, the Einstein–Roscoe model, although widely used, is insufficient to reproduce the viscosity data of heterogeneous molten coal ash slag. This drawback is because the model does not take into account the dependence of apparent viscosity on the shear rate and rheological parameters, including shear rate and yield stress.

To consider the effect of the change in the complex rheology of the crystal-bearing molten coal ash slag on the viscosity, the increase in shear stress as a function of increasing shear rate is described using a modified version of the semiempirical Eq. 17[67]

$$\tau_w = \dot{\gamma}\,\eta_\infty + \frac{(\eta_0 - \eta_\infty)\,\dot{\gamma}}{1 + \dot{\gamma}\,(\eta_0 - \eta_\infty)/C} + \tau_y \qquad (17)$$

where η_0 and η_∞ are the viscosities at the lowest and highest shear rates, respectively. Parameter C can be calculated from

$$C = \left(\frac{\phi_{max}^2}{\phi_{max} - \phi}\right)\left(\frac{\eta_l^2}{D_P^2 \rho \tau_y}\right)^{0.21} \tau_y \qquad (18)$$

where η_l is the viscosity of the homogeneous melt, ϕ_{max} is the maximum solid-packing fraction. D_P is the mean diameter of the crystal particles, as obtained through morphological analysis of the crystals in the samples, and ρ is the density of the fluid, which is estimated at 2400 kg m^{-3}. Figure 13 shows the experimental data of the viscosity of sample Nos. 6–30 at the lowest and highest shear rates within the 1370–1280°C temperature range.

To make a prediction on the viscosity of the molten coal ash slag at different times and constant temperature using

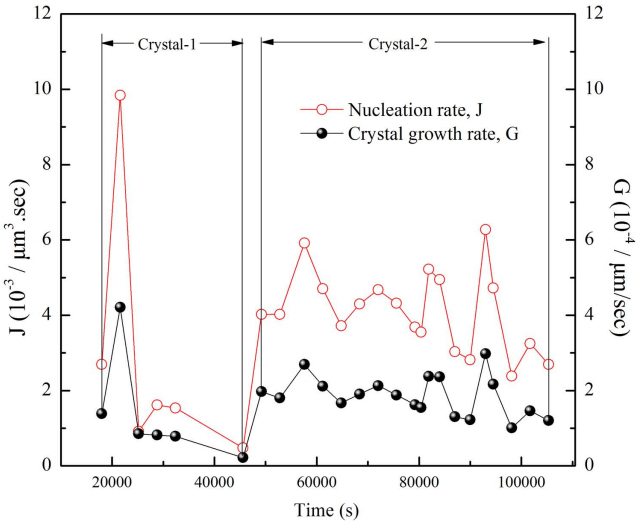

Figure 12. Nucleation rate and growth rate of crystals in the molten coal ash slag.

Nucleation rate as determined by the absolute value of the slope of the CSD plot. Crystal growth rate as determined by the intercept of the CSD plot. [Color figure can be viewed in the online issue, which is available at wileyonlinelibrary.com]

the modified model, the effect of the nucleation and growth rates of the crystals on the crystal content with changing time is considered. The number of crystals and the dimensions they can reach in the molten silicate liquid depend on the cooling history and changes according to the time of appearance. From Eq. 16, the number density n_i of a crystal

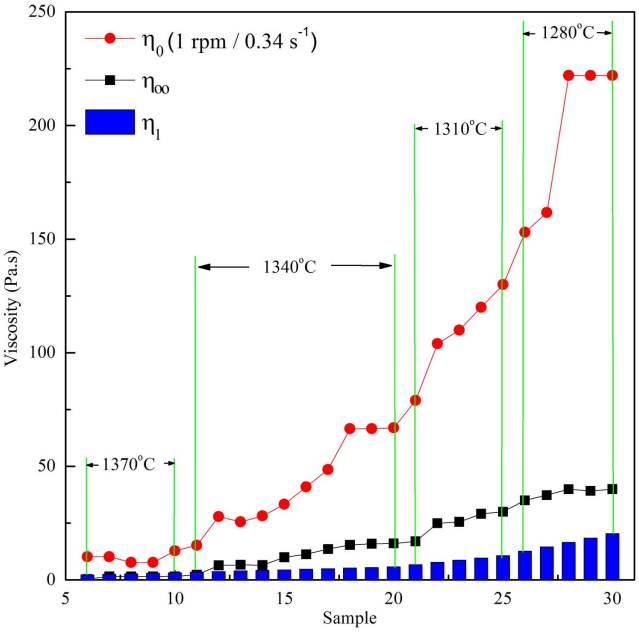

Figure 13. The measured viscosity at the lowest and highest shear rates, and the calculated viscosity of the remaining liquid phase by FactSage in the molten coal ash slag samples Nos. 6–30, at the 1370–1280°C temperature range.

[Color figure can be viewed in the online issue, which is available at wileyonlinelibrary.com]

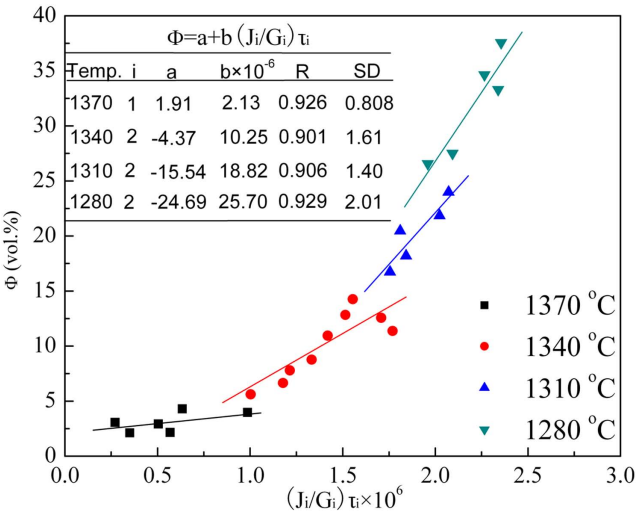

Figure 14. Crystal volume fraction as a function of the $(J_i/G_i)\bullet\tau_i$ term.

[Color figure can be viewed in the online issue, which is available at wileyonlinelibrary.com]

of size L_i at time τ_i is equal to the nucleation density at time τ_{L_i} when they appeared[68]

$$n_i(\tau_i, L_i) = \frac{J_i(\tau_{L_i})}{G_i(\tau_{L_i})} (i = 1, 2) \tag{19}$$

where τ_{L_i} is the time at which the crystal phase i of the class around L_i at time τ_i grew from 0 to L_i within the interval $t_i - t_{L_i}$. $n_i(\tau_i, L_i)$, $J_i(\tau_{L_i})$, and $G_i(\tau_{L_i})$ are the crystal population density, nucleation rate, and growth rate of crystal phase i, respectively, at the time of appearance of the crystals of dimension L_i and that of a previous volume over the actual volume. The crystal volume fraction and crystal population density at different times are then correlated (Figure 14). Thus, the crystal volume fraction can be calculated from the following equation

$$\phi = a + b\frac{J_i}{G_i} \cdot \tau_i \tag{20}$$

The sum of the squared differences of crystal volume fraction and the $(J_i/G_i) \cdot \tau_i$ term was minimized by adjusting the parameters a and b under different temperatures. The parameters obtained for this set of samples are shown in Figure 14.

The differences in the microstructures of the suspension at different shear rates lead to the inappropriateness of using the single model to predict viscosity under different shear rates.[69] Therefore, on the basis of the Einstein–Roscoe and Pinkerton models, η_0 and η_∞ of the viscosity of the molten coal ash slag samples at the lowest and highest shear rates can be calculated by correlating the experimental values of η_0 and η_∞ with the $\eta_l\left(\frac{\phi_{\max}}{\phi_{\max}-\phi}\right)^{2.5}$ and $\eta_l e^{\left[\left(2.5+\left(\frac{\phi}{\phi_{\max}-\phi}\right)^{0.48}\right)\frac{\phi}{\phi_{\max}}\right]}$ terms,[70] respectively (Figure 15)

$$\eta_0 = 15.45 + 3.28\eta_l\left(\frac{\phi_{\max}}{\phi_{\max}-\phi}\right)^{2.5} \tag{21}$$

$$\eta_\infty = 3.72 + 0.75\eta_l e^{\left[\left(2.5+\left(\frac{\phi}{\phi_{\max}-\phi}\right)^{0.48}\right)\frac{\phi}{\phi_{\max}}\right]} \tag{22}$$

In the literature, the $\phi_{\max}$ values range from 0.4 to 0.74, with a classical value of 0.66 for a silicate material. Thus,

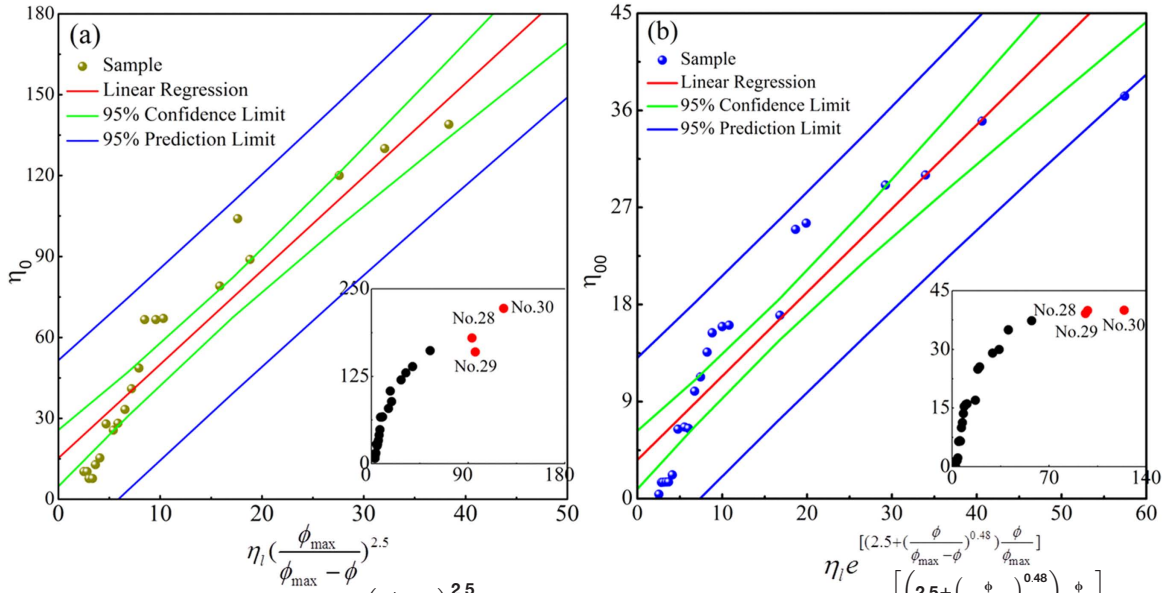

Figure 15. (a) η_0 as a function of the $\eta_l\left(\frac{\phi_{max}}{\phi_{max}-\phi}\right)^{2.5}$ term. (b) η_∞ as a function of the $\eta_l e^{\left[\left(2.5+\left(\frac{\phi}{\phi_{max}-\phi}\right)^{0.48}\right)\frac{\phi}{\phi_{max}}\right]}$ term.

[Color figure can be viewed in the online issue, which is available at wileyonlinelibrary.com]

the value of ϕ_{max} in Eqs. 21 and 22 is defined as 0.66. The viscosity of the liquid phase (η_l) is obtained using FactSage (Figure 13). The parameter C was calculated using Eq. 18, and the results are shown in Figure 16a.

Finally, the modified model systems, Eqs. 17–22, were used to predict the viscosity of the molten coal ash slag sample Nos. 6–30. A plot of the measured vs. the predicted viscosities is shown in Figure 16b. Most of the samples (except samples Nos. 28–30) are clearly deformed, indicating that the rheological properties calculated using this method, agree closely with the measured values. However, the measured viscosity results show obvious deviations from the estimated value for the samples Nos. 28–30. The possible causes are the experiment errors and model accuracy. The three samples formed a rheologically complicated system when the temperature decreased to 1280°C, which led the factors of the thermal, electrical, and hydrodynamic interactions of systems, and wall slip effect affect the viscosity and can make unreasonable viscosity approximations at the lowest and highest shear rates in Eqs. 21 and 22.

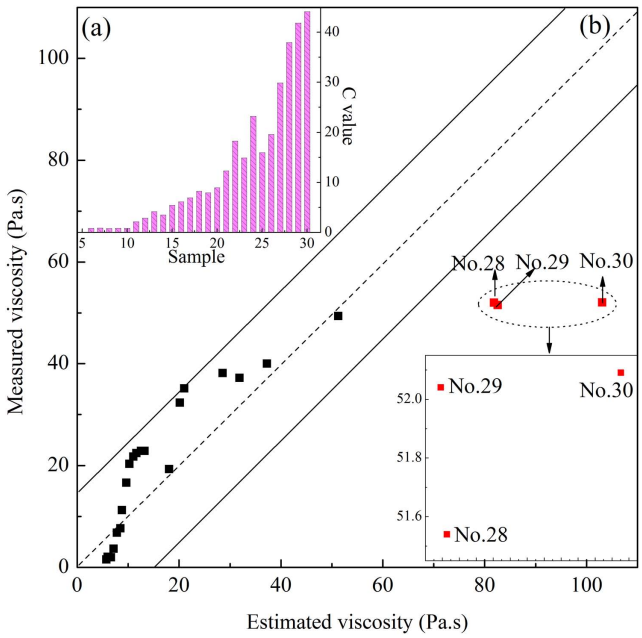

Figure 16. (a) Values of parameter C for sample Nos. 6–30.

(b) Plot of the measured viscosities vs. the viscosities estimated under our experimental conditions. [Color figure can be viewed in the online issue, which is available at wileyonlinelibrary.com]

Conclusions

Viscosity measurements on the molten coal ash slag suspensions containing up to 35.51 vol % of crystals were performed in the 1280–1400°C temperature range. The effect of crystal concentration, shear rate, time, and temperature on the rheological behavior of the molten coal ash slag was explored, and these parameters were included as variables in a modified power law that fits our data. The CSD method was applied to analyze quantitatively the textures of the molten coal ash slag sample at various stages; the results provide information on the rates of *in situ* crystal nucleation and growth.

The experiments reported here demonstrate that the introduction of suspended crystals in the melt increases the viscosity and enhances the shear rate-dependent rheology, resulting in the time dependence of the viscosity, flow pattern, and yield stress before the thermodynamic equilibrium in the cooling processes is reached. The molten coal ash slag contained crystal content higher than 4.70 vol % and displayed dramatical non-Newtonian behaviors, such as shear-thinning, with decreasing temperature. These behaviors became increasingly obvious as the crystal content is increased.

The specific CSD plots of crystals from 25 samples were examined to establish their growth conditions. Some crystal samples exhibit curves such as concave down shapes, instead of a straight line. The crystal growth mechanism and system stability responsible for the nonlinearity of the CSD plots

may be due to surface-controlled crystal growth, followed by an episode of textural coarsening. The crystal nucleation and growth rates determined through the use of the CSD method suggest that crystallization occurred through very short undercooling throughout the crystallization interval.

Finally, the modified models systems of Eqs. 17–22 describe the complex rheological behavior of crystals in the molten coal ash slag. These equations provide the basis for the evaluation of the effect of microscale crystallization processes that occur during cooling on the macroscopic behavior of the molten coal ash slag.

Acknowledgments

The authors thank Prof. Xuedong Zhu, Prof. Qi Zhang, Dr. Fachun Jiao, and Dr. Yin Meng of Chubu University, the editors and five anonymous reviewers who carefully looked through this manuscript, discussed, improved, and rendered it to its actual state. The authors express gratitude to other members of Coal Gasification Laboratory who also contributed and helped in this research program, including Dr. Lu Liu, Dr. Haojun Lu, and Ms. Yimin Sun.

Notation

G_i = growth rate of crystal phase i, μm/s
J_i = nucleation rate of crystal phase i, $\mu m^3/s$
L_i = characteristic crystal size, mm
L_i^* = maximum length of crystal phase i, mm
n_i = population density of crystal phase i, number/mm^3
n_i^0 = population density of nucleus-size crystals, number/mm^3
N_i = total number of crystal phase i

Greek letters

$\dot{\gamma}$ = shear rate, s^{-1}
$\Delta\dot{\gamma}$ = Change of the shear rate, s^{-1}
η_B = coefficients of the Bingham model, Pa s
η_N = coefficients of the Newtonian model, Pa s
η_s = apparent viscosity, Pa s
$\eta_{s,final}$ = viscosity at the final cooling condition in the viscosity measurement, Pa s
$\eta_{s,initial}$ = viscosity at the initial cooling condition in the viscosity measurement, Pa s
$\Delta\eta_{\dot{\varepsilon}}$ = change rate of viscosity with respect to shear rate, Pa s^2
$\eta_{\dot{\varepsilon},initial}$ = viscosity at the initial condition in the shear-thinning measurement, Pa s
$\eta_{\varepsilon,finial}$ = viscosity at the final condition in the shear-thinning measurement, Pa s
η_0 = viscosity at the lowest shear rate in the flow pattern measurement, Pa s
η_∞ = viscosity at the highest shear rate in the flow pattern measurement, Pa s
η_l = viscosity of remaining liquid phase in the molten coal ash slag, Pa s
τ_w = shear stress, Pa
τ_Y = yield stress, Pa
$\Delta\tau_Y$ = relative increase in yield stress, dimensionless
$\tau_{Y,initial}$ = yield stress at the initial condition in the yield stress measurement, Pa
$\tau_{Y,final}$ = yield stress at the final condition in the yield stress measurement, Pa
τ_i = average residence time of crystal phase i, s
ϕ = crystal volume fraction, vol %
ϕ_{max} = maximum solid packing fraction, dimensionless

Literature Cited

1. U.S. Energy Information Administration. Annual Energy Review 2011. Washington, DC, 2011.
2. Sheppard MC, Socolow RH. Sustaining fossil fuel use in a carbon-constrained world by rapid commercialization of carbon capture and sequestration. *AIChE J*. 2007;53:3022–3028.
3. Davison J. Performance and costs of power plants with capture and storage of CO_2. *Energy*. 2007;32:1163–1176.
4. Figueroa JD, Fout T, Plasynski S, McIlvried H, Srivastava RD. Advances in CO_2 capture technology–the U.S. department of energy's carbon sequestration program. *Int J Greenh Gas Con*. 2008;2:9–20.
5. Barnes I. IGCC Roadmaps for the Asia-Pacific Region. London: IEA Clean Coal Center, 2009.
6. Davidson R, Santos S. Oxy-Fuel Combustion of Pulverised Coal. London: IEA Clean Coal Center, 2010.
7. Song W, Tang L, Zhu X, Wu Y, Rong Y, Zhu Z, Koyama S. Fusibility and flow properties of coal ash and slag. *Fuel*. 2009;88:297–304.
8. Bryers RW. Fireside slagging, fouling, and high-temperature corrosion of heat-transfer surface due to impurities in steam-raising fuels. *Prog Energ Combust*. 1996;22:29–120.
9. Coletti F, Ishiyama EM, Paterson WR, Wilson DI, Macchietto S. Impact of deposit aging and surface roughness on thermal fouling: distributed model. *AIChE J*. 2010;56:3257–3273.
10. van der Drift A, Boerrigter H, Coda B, Cieplik MK, Hemmes K. Entrained Flow Gasification of Biomass. Petten: ECN, 2004.
11. Johnson EK. A non-Newtonian flow model for coal ash slag. *J Eng Gas Turb Power*. 1984;106:777–781.
12. Browning GJ, Bryant GW, Hurst HJ, Lucas JA, Wall TF. An empirical method for the prediction of coal ash slag viscosity. *Energy Fuels*. 2003;17:731–737.
13. Song W, Dong Y, Wu Y, Zhu Z. Prediction of temperature of critical viscosity for coal ash slag. *AIChE J*. 2011;57:2921–2925.
14. Boow J. Viscosity/temperature characteristic of some Australian coal ash slags in the range 1100 to 1600°C. *J I Fuel*. 1965;3:5–12.
15. Watt JD, Fereday F. The flow properties of slags formed from the ashes of British coals: part 1. Viscosity of homogeneous liquid slags in relation to slag composition. *J I Fuel*. 1969;42:99–103.
16. Watt JD, Fereday F. The flow properties of slags formed from the ashes of British coals: part 2. The crystallizing behavior of the slags. *J I Fuel*. 1969;42:131–134.
17. Schobert HH, Streeter RC, Diehl EK. Flow properties of low-rank coal ash slags. *Fuel*. 1985;64:1611–1617.
18. Jung B, Schobert HH. Improved prediction of coal ash slag viscosity by thermodynamic modeling of liquid-phase composition. *Energy Fuels*. 1992;6:387–398.
19. Nowok JW, Hurley JP, Stanley DC. Local structure of a lignitic coal ash slag and its effect on viscosity. *Energy Fuels*. 1993;7:1135–1140.
20. Nowok JW. Viscosity and structural state of iron in coal ash slags under gasification conditions. *Energy Fuels*. 1995;9:534–539.
21. Hurst HJ, Patterson JH, Quintanar A. Viscosity measurements and empirical predictions for some model gasifier slags–II. *Fuel*. 2000;79:1797–1799.
22. Hurst HJ, Novak F, Patterson JH. Viscosity measurements and empirical predictions for fluxed Australian bituminous coal ashes. *Fuel*. 1999;78:1831–1840.
23. Kondratiev A, Jak E. Predicting coal ash slag flow characteristics. *Fuel*. 2001;80:1989–2000.
24. Kær SK, Rosendahl LA, Baxter LL. Towards a CFD-based mechanistic deposit formation model for straw-fired boilers. *Fuel*. 2006;85:833–848.
25. Groen JC, Brooker DD, Welch PJ, Oh MS. Gasification slag rheology and crystallization in titanium-rich, iron-calcium-aluminosilicate glasses. *Fuel Process Technol*. 1998;56:103–127.
26. Mudersbach D, Drissen PM, Kuhn M, Geiseler J. Viscosity of slags. *Steel res*. 2001;72:86–90.
27. Oh MS, Brooker DD, de Paz EF, Brady JJ, Decker TR. Effect of crystalline phase formation on coal slag viscosity. *Fuel Process Technol*. 1995;44:191–199.
28. Song W, Sun Y, Wu Y, Zhu Z, Koyama S. Measurement and simulation of flow properties of coal ash slag in coal gasification. *AIChE J*. 2011;57:801–818.
29. Einstein A. Eine neue bestimmung der moleküldimensionen. *Ann Phys*. 1911;34:591–592.
30. Roscoe R. The viscosity of suspensions of rigid spheres. *Br J Appl Phys*. 1952;3:267–269.
31. Pinkerton H, Stevenson RJ. Methods of determining the rheological properties of magmas at sub-liquidus temperatures. *J Volcanol Geotherm Res*. 1992;53:47–66.
32. Marsh BD. On the crystallinity, probability of occurrence, and rheology of lava and magma. *Contrib Mineral Petr*. 1981;78:85–98.

33. De Yoreo JJ, Vekilov PG. Principles of crystal nucleation and growth. *Rev Mineral Geochem.* 2003;54:57–93.
34. Marsh BD. Crystal size distribution (CSD) in rocks and the kinetics and dynamics of crystallization. *Contrib Mineral Petr.* 1988;99:277–291.
35. Cashman KV, Marsh BD. Crystal size distribution (CSD) in rocks and the kinetics and dynamics of crystallization II: Makaopuhi lava lake. *Contrib Mineral Petr.* 1988;99:292–305.
36. Massoudi M, Wang P. A Brief Review of Viscosity Models for Slag in Coal Gasification. Pittsburgh: U.S. Department of Energy, 2011.
37. Song W, Tang L, Zhu X, Wu Y, Zhu Z, Koyama S. Flow properties and rheology of slag from coal gasification. *Fuel.* 2010;89:1709–1715.
38. Lejeune AM. Richet P. Rheology of crystal-bearing silicate melts: an experimental study at high viscosities. *J Geophys Res.* 1995;100:4215–4229.
39. Fryda L, Sobrino C, Cieplik M, Van De Kamp WL. Study on ash deposition under oxyfuel combustion of coal/biomass blends. *Fuel.* 2010;89:1889–1902.409.
40. Yong SZ, Gazzino M, Ghoniem A. Modeling the slag layer in solid fuel gasification and combustion-Formulation and sensitivity analysis. *Fuel.* 2012;92:162–170.
41. Tonmukayakul N, Nguyen QD. A new rheometer for direct of measurement of the flow properties of coal ash at high temperatures. *Fuel.* 2002;81:397–404.
42. Wang S, Ravindranath S, Boukany PE. Homogeneous shear, wall slip, and shear banding of entangled polymeric liquids in simple-shear rheometry: a roadmap of nonlinear rheology. *Macromolecules.* 2011;44:183–190.
43. Muckenfuss S. Wall Effects in Shear-Flowing Suspensions. Göttingen: Cuvillier Verlag, 2006.
44. Kumar AA, Medhi BJ, Singh A. Measurement of apparent wall slip velocity in concentrated suspension of non-colloidal particles in open channel flow. In: 7th International Conference on Multiphase Flow. Tampa, FL, USA, 2010.
45. Walls HJ, Caines SB, Sanchez AM, Khan SA. Yield stress and wall slip phenomena in colloidal silica gel. *J Rheol.* 2003;47:847–868.
46. Nguyen QD, Boger DV. Yield stress measurement for concentrated suspensions. *J Rheol.* 1983;27:321–349.
47. Yoshimura AS, Prud'homme RK, Princen HM, Kiss AD. A comparison of techniques for measuring yield stresses. *J Rheol.* 1987;31:699–710.
48. Jana SC, Kapoor B, Acrivos A. Apparent wall slip velocity coefficients in concentrated suspensions of noncolloidal particles. *J Rheol.* 1995;39:1123–1132.
49. Russel WB, Grant MC. Distinguishing between dynamic yielding and wall slip in a weakly flocculated colloidal dispersion. *Colloids Surface A.* 2000;161:271–282.
50. Nowok JW. Viscosity and phase transformation in coal ash slags near and below the temperature of critical viscosity. *Energy Fuels.* 1994;8:1324–1336.
51. Higgins MD. A crystal size-distribution study of the Kiglapait layered mafic intrusion, Labrador, Canada: evidence for textural coarsening. *Contrib mineral Petr.* 2002;144,314–330.
52. Higgins MD. Magma dynamics beneath Kameni volcano, Thera, Greece, as revealed by crystal size and shape measurements. *J Volcanol Geotherm Res.* 1996;70:37–48.
53. Higgins MD. Closure in crystal size distributions (CSD), verification of CSD calculations, and the significance of CSD fans. *Am Mineral.* 2002;87:171–175.
54. Saltykov SA. The determination of the size distribution of particles in an opaque material from a measurement of the size distribution of their sections. In: Elias H, editor. Stereology, Berlin-Heidelberg-NewYork: Springer, 1967:163–73.
55. Bindeman IN. Crystal sizes in evolving silicic magma chambers. *Geology.* 2003;31:367–370.
56. Bale CW, Chartrand P, Degterov SA, Eriksson G, Hack K, Mahfoud RB, Melancon J, Pelton AD, Petersen S. FactSage thermochemical software and databases. *Calphad.* 2002;26:189–228.
57. Middleman S. The Flow of High Polymers: Continuum and Molecular Rheology. NewYork: Interscience Publishers, 1968.
58. Bird RB, Armstrong RC, Hassager O. Dynamics of Polymeric Liquids. NewYork: Wiley, 1987.
59. Nzihou A, Attias L, Sharrock P, Ricard A. A rheological, thermal and mechanical study of bone cement-from a suspension to a solid biomaterial. *Powder Technol.* 1998;99:60–69.
60. Bottinga Y, Richet P. Silicate melt structural relaxation: rheology, kinetics, and Adam-Gibbs theory. *Chem Geol.* 1996;128:129–141.
61. Mason TG. New fundamental concepts in emulsion rheology. *Curr Opin Colloid In.* 1999;4:231–238.
62. Bournonville B, Nzihou A. Rheology of non-Newtonian suspensions of fly ash: effect of concentration, yield stress and hydrodynamic interactions. *Powder Technol.* 2002;128:148–158.
63. Barnes HA, Hutton JF, Walters K. An Introduction to Rheology. Amsterdam: Elsevier, 1989.
64. Pinkerton H, Norton G. Rheological properties of basaltic lavas at sub-liquidus temperatures: laboratory and field measurements on lavas from Mount Etna. *J Volcanol Geotherm Res.* 1995;68:307–323.
65. Lofgren G. Experimental studies on the dynamic crystallization of silicate melts. In: Hargraves RB, editor. Physics of Magmatic Processes. Princeton, New Jersey: Princeton University Press, 1980:487–551.
66. Berglund KA, Kaufman EL, Larson MA. Growth of contact nuclei of potassium nitrate. *AIChE J.* 1983;29:867–869.
67. Gay EC. Nelson PA, Armstrong WP. Flow properties of suspensions with high solids concentration. *AIChE J.* 1969;15:815–822.
68. Armienti P, Pareschi MT, Innocenti F, Pompilio M. Effects of magma storage and ascent on the kinetics of crystal growth. *Contrib Mineral Petr.* 1994;115:402–414.
69. Barnes HA, Hutton JF, Walters K. An Introduction to Rheology. NewYork: Elsevier, 1989.
70. Champallier R, Bystricky M, Arbaret L. Experimental investigation of magma rheology at 300 Mpa: from pure hydrous melt to 76 vol.% of crystals. *Earth Planet Sci Lett.* 2008;267:571–583.

Manuscript received Jun. 13, 2012, and revision received Jan. 16, 2013.